New Generation Perovskite Solar Cells with Solution-Processed Perylene-Diimide Derivative as Electron-Transport Layer

Hua Zhang,[a,+] *Lingwei Xue,*[b,+] *Junbo Han,*[c] *Yong Qing Fu,*[d] *Yan Shen,*[a] *Zhi-Guo Zhang,*[b*] *Yongfang Li,*[b] *Mingkui Wang,*[a*]

[a] Wuhan National Laboratory for Optoelectronics, Huazhong University of Science and Technology, Luoyu Road 1037, Wuhan, 430074, P. R. China

[b] CAS Key Laboratory of Organic Solids, Institute of Chemistry, Chinese Academy of Sciences, Beijing 100190, P. R. China

[c] Wuhan National High Magnetic Field Center, Huazhong University of Science and Technology, 1037 Luoyu Road, Wuhan 430074, Hubei, P. R. China

[d] Department of Physics and Electrical Engineering, Faculty of Engineering and Enviornment, Northumbria University, Newcastle Upon Tyne, NE1 8ST, UK.

[+] Contributed equally.

KEYWORDS: Perovskite solar cell; Hole-blocking material; Low-temperature solution-processing; Planar-heterojunction; Small molecular semiconductors; Electron-Transport Layer

Abstract:

In this research work, for the first time, we introduced amino-substituted perylene diimide derivative (N-PDI) as an alternative electron transport layer (ETL) to replace the commonly used TiO2 in planar heterojunction perovskite solar cells. Two types of device structures i.e., glass/FTO/N-PDI/CH3NH3PbI3-xClx/spiro-MeOTAD/Au, and polyethylene terephthalate (PET)/ITO/N-PDI/CH3NH3PbI3-xClx/spiroMeOTAD/Au, were fabricated on both rigid and flexible substrates using room-temperature solution processing technique. Based on the proposed device structures, the power conversion efficiency (PCE) of 17.66% was obtained based on glass/FTO rigid substrates, and a PCE of 14.32% was achieved based on PET/ITO flexible substrates. Results revealed that the terminal amino group in N-PDI resulting in the enhanced wetting capability of surfaces to perovskite, and the lower the surface work function of FTO substrate as well as passivate the surface trap states of perovskite films. Our results confirm that small molecule semiconductor N-PDI can serve as an effective 15 electron-transport material for achieving high-performance perovskite solar cells and draw molecular design guidelines for electronselective contacts with perovskite.

1. Introduction

In the past five years, there is tremendous development in the field of perovskite solar cells (PVSCs) with advantages of low cost, simple fabrication, and high efficiency.[1-4] To date, the certified value of maximum power conversion efficiency (PCE) for the PVSCs is 20.1%.[5] The PVSCs, based on either the mesoscopic or the planar structure architectures, are typically composed of a transparent electrode, a metal electrode, a light harvesting perovskite layer sandwiched between electron transport layer (ETL) and hole transport layer (HTL). The interfaces among these layers are crucial for the PVSC devices delivering a high open-circuit voltage (V_{OC}). They determine effective carrier separation and suppress charge recombination at the front contact with?? transparent conducting oxides such as fluorine-doped tin oxide (FTO) or indium-doped tin oxide coated glass, as well as back contact of typically metals such as Ag or Au. For the conventional PVSCs (i.e., n-i-p), the most used ETL and HTL materials reported in literature are TiO_2 and 2,2',7,7'-tetrakis-(N,N-di-pmethoxyphenylamine)-9,9'-spirobifluorene (spiro-OMeTAD), respectively [XX]. Spiro-OMeTAD becomes a good HTL material for highly efficient solid-state cells due to its longer charge recombination lifetime compared to the other HTLs.[6] While the TiO_2 is an excellent ETL due to its higher electron mobility and suitable energy levels of conduction and valence bands.[1, 3, 7]

In addition to TiO_2, several other metal oxides, including ZnO, [8-14] In_2O_3, [15-20] and SnO_2, [21-28] exhibit similar or even better electronic and optical properties than those of the TiO_2. Theoretically, these oxides could act as good ETL materials as the TiO_2. For example, PVSCs using SnO_2 as the ETL have achieved hysteresis-free PCEs of over 18%.[28] However, utilization of inorganic ETLs particularly the TiO_2 still requires a high-temperature process to increase the crystallinity and achieve a high charge carrier mobility. [29] High-temperature sintering has many drawbacks because it not only results in increased cost and slow production, but also limits usages of temperature-resilient substrates, and thus prevents the utilization of plastic and malleable metal foils as well as multi-junction device architectures.[30] Therefore, replacing the sintered ETLs with new material and process can promote the successful

applications of perovskite photovoltaic technology into wide fields, such as organic photovoltaics. Several reports have already shown that many materials can act as effective ETLs in the PVSCs with a similar performance compared with those fabricated through high-temperature sintering process, and these includelow-temperature processed graphene/TiO_2 nanocomposites, [31] yttrium doped TiO_2, [2] atomic layer deposited SnO_2 [28] and PbI_2 in a $CH_3NH_3PbI_3$ film prepared using a two-step method [32] as well as the ultraviolet (UV)-ozone treated FTO electrode. [33] These studies highlighted the promising direction of developing solution-processed ETLs for the PVSCs, with advantages including enhanced simplicity, low-temperature solution process for device optimization and multi-junction construction.

In this study, low-temperature solution-processed n-type organic semiconductors will be investigated as the ETLs as an alternative new approach. Compared with its inorganic counterparts, the organic ETLs have advantage of tuability of photo-physic properties by structural changes; availability of multi-defined structures, easy purification and synthesis in material processing, as well as batch-to-batch reproducibility and flexibility. Recent studies on the organic ETLs have identified that it should passivate the trap states of perovskite active film in order for what? [??]. However, due to the poor understanding of the interaction between the perovskite layer and the organic materials, few organic materials have been successfully used as the ETLs. Although currently *full name??? of* PCBM was regarded as one successful example [],its high price and photochemical instability limits its successful commercial application.

In this paper, we demonstrated, for the first time, the possibility of utilizing an n-type organic semiconductor PDIN (perylene diimide derivative, see Figure 1a) as the ETL in the PVSCs with an n-i-p structure () of FTO/PDIN/$MAPbI_{3-x}Cl_x$/spiro-OMeTAD/Au. The exploration of perylene diimide derivative as the ETL was inspired by their several fascinating properties, including photochemical stability, high electron affinities, easy functionalization and high conductivities. The multiple functionalities of this newly developed PDIN, including lowering the work function of FTO, appropriate energy levels, resistance to aprotic

polar solvents, high conductivity, and most importantly, passivating the trap states of the perovskite, etc., render it as an excellent ETL in a standard device structure. Based on a low-temperature process to fabricate the PDIN, we demonstrated that a very competitive PCE of 16.17% on rigid substrates and 11.24% on flexible substrates can be achieved under simulated irradiation of AM 1.5G at 100 mW cm^{-2}.

2. RESULTS AND DISCUSSION

2.1 Device structure and fabrication

Figure 1a shows the device structure of the standard planar heterojunction of the PVSCs having the PDIN as the ETL. The developed PDIN is easily achievable using environmentally friendly reagents. The PDIN is alcohol- or water-soluble if adding acetic acid (2% in volume), whereas it is insoluble in chlorinated solvents, such as chlorobenzene. Benefitted from the extended planar structures of the PDI units and the polar aliphatic amino group, the PDIN shows a high conductivity (0.8×10^{-5} S cm^{-1}) and exhibits good performance as a cathode buffer layer in organic solar cells. [34] When the PDIN solution was used as a cathode buffer layer in an inverted device structure (p-i-n) to reduce the energy offset between the Fermi levels of Ag and LUMO (the lowest unoccupied molecular orbital) of fullerene derivative (PCBM), we found the degradation of the perovskite layer due to the acetic acid inside the PDIN solution. Therefore, a similar XXX, PDINO, with amino *N*-oxide group, soluble in methanol without the assistant of acid, was applied as cathode buffer layer in inverted structure. [35] Also due to insolublity of the PDIN and PDINO in the chlorinated solvents, it is impossible to apply them as the ETL (replacing the PCBM) to simply the device structure. However, for a conventional device structure, the resistance of the PDIN in aprotic polar solvents, such as *N,N*-Dimethyl-formamide (DMF) and dimethyl sulfoxide (DMSO), can solve this problem due to its orthogonal polarity for each successive layer, thus it inspired us to exploit the PDIN as a potentially cost effective ETL for the PVSCs.

The PDIN film can survive the DMF rinse and is stable in both DMF and methanol.

To fabricate the device, the $CH_3NH_3PbI_{3-x}Cl_x$ ($MAPbI_{3-x}Cl_x$, $CH_3NH_3^+$ being abbreviated as MA thereafter) films were directly deposited onto the substrate coated with PDIN?? using a one-step spin-coating method, resulting in the absence of any PbI_2 phase in the perovskite film as evidenced by x-ray diffraction (XRD) analysis (Figure S1). Following the deposition of the $MAPbI_{3-x}Cl_x$ layer, a spiro-OMeTAD HTL (~150 nm) was deposited by spin coating. The cells were finished with thermally evaporated Au back contacts. The corresponding energy level diagram of the device is illustrated in Figure 1b. Since the LUMO level of the PDIN aligns well with the conduction band (CB) of the $MAPbI_{3-x}Cl_x$, it serves as a good ETL to energetically promote electron extraction but effectively block holes at the PDIN/$MAPbI_{3-x}Cl_x$ interface. Furthermore, the amino group of the PDIN produces large interfacial dipoles at the FTO/PDIN interface which induces a vacuum-level shift and modifies the work function of FTO electrode. [36] This was verified using ultraviolet photoelectron spectroscopy (UPS), which revealed the electronic properties of PDIN interlayer on the FTO substrate as illustrated in Figure 2a. After deposition of an ultrathin layer (8 nm) of the PDIN, the work function of FTO was reduced to 4.0 eV from its original 4.4 eV, which facilitates an efficient electron transport between the ETL and FTO electrode. The excellent light transparency of the interlayer is also essential for avoiding overlap and parasitical absorption of the $MAPbI_{3-x}Cl_x$ to achieve high-performance PVSCs.

Figure 2b shows the optical transmittance and absorption spectra of the PDIN films with different thicknesses. As can be seen, the FTO/PDIN substrate exhibits an absorption in the range between 450 and 600 nm. As a result, the FTO/PDIN possesses a less transmittance than the bare FTO in this range. While the UV-vis absorbance spectrum of the $MAPbI_{3-x}Cl_x$ based on a layer (8 nm) of the PDIN substrate has no apparent difference compared to that based on compact TiO_2 (Figure S2). This should be due to the higher absorption coefficient of perovskite in comparison with the conventional organic molecules. [37]

Steady-state photoluminescence (PL) and time-resolved PL decay of the $MAPbI_{3-x}Cl_x$ film on different substrates were further conducted to investigate the

charge extraction efficiency of the ETL. An excitation wavelength of 532 nm with a penetration depth of ~ 80 nm (much less than the perovskite film thickness of ~300 nm), was used to excite the perovskite films either from the FTO side or from the air side, and the PL from the perovskite films with and without ETLs were measured. As illustrated in Figure 2c, both perovskite films with TiO_2 as ETL and without TiO_2 showed a PL peak at 778 nm, which were independent to the directions of the incident lights. Whereas, the perovskite film with the PDIN as the ETL had a blue-shift PL peak from 778 to 770 nm when the FTO side was excited, and this peak was considered as signature of filling the trap states of perovskite. This enables the recovery of the bandgap.[38] Therefore we suggest that the PDIN can passivate the trap states of the perovskite by using the terminal amino group. This conclusion agrees well with the similar passivation effect of amino-functionalized conjugated polymer reported by Sun *et al*.[39] Moreover, the perovskite film based on the FTO/PDIN substrate exhibits a higher degree of PL quenching compared to that based on the FTO/TiO_2 substrate either from the FTO side or from the air side, indicating that the PDIN can extract electrons more efficient from perovskite absorber. The enhanced electron extraction should be the result of the passivation effect of PDIN and better matched energy levels between the conduction bands of the PDIN and $MAPbI_{3-x}Cl_x$ as previously discussed. The efficient PL quenching of the PDIN was also verified by studying the charge carrier lifetime of $MAPbI_{3-x}Cl_x$, which could be estimated from the time-resolved PL decay (Figure 2d). The PL lifetimes are determined by the single-exponential fits to the PL decay. [40, 41] The PL lifetime of the $MAPbI_{3-x}Cl_x$ on the FTO substrate was estimated to be 18.05 ns, while it decreased to 14.58 ns and 12.76 ns when it was applied on top of TiO_2 and PDIN, respectively. This indicates that faster and more efficient carrier extraction was achieved at the PDIN/perovskite interface.

2.2 Device characterization

The conventional PVSCs with configuration of FTO/PDIN/$MAPbI_{3-x}Cl_x$/spiro-OMeTAD/Au were fabricated accordingly (Figure 1a) and characterized. The

detailed fabrication procedures of these devices were described in the experimental section. Figure 3a presents the current density vs. voltage (J-V) curves of the PVSCs based on PDIN with different thicknesses, obtained in a reverse scan (from the V_{OC} to the J_{SC}) at a scan rate of 20 mV per step with a delay time of 0.005 s. Their corresponding photovoltaic parameters are summarized in Tables 1 and 2. Encouragingly, the optimized PVSC devices with the PDIN thickness of 8 nm exhibited an impressive PCE_{MAX} value of 16.17%, whereas the control TiO_2-based device (as explained in XX?) yielded a PCE_{MAX} value of 15.03%. The value of V_{OC} was increased from 1.05 V to 1.08 V, and can be attributed to a better energy alignment at the FTO/ETL and ETL/perovskite interfaces. The passivation effect of the PDIN can also decrease the trap states and increase the carrier extraction. These minimize the potential loss and enlarge the built-in potential across the interface in the device. In addition to the V_{OC}, significant increase of both values of J_{SC} (from 20.45 to 20.80 mA cm^{-2}) and FF (from 0.70 to 0.72) were also obtained in the PVSCs using the PDIN interlayer with a thickness of 8 nm. The enhanced J_{SC} and FF can be attributed to the combined effects of efficient electron extraction and hole blocking of the PDIN compared to the controlled device made from the high-temperature treated TiO_2.

The reproducibility of 20 FTO/PDIN-based devices was evaluated and the obtained histogram showing PCE distribution of over 20 devices is shown in Figure S3. An average PCE value of 15.5% was achieved with half of the devices showing the PCE values over 15%. The results showed clearly the good reproducibility of the FTO/PDIN-based device. Figure 3b shows results of the incident photon-to-current conversion efficiency (IPCE) of the PVSCs based on the FTO/PDIN devices, which have a higher photon-to-electron conversion efficiency than that of the FTO/TiO_2-based device in the wavelength range tween 600 and 750 nm. Results from the dark current characterization of the PVSCs showed that the FTO/PDIN-based device possesses a lower leakage current density compared with the FTO/TiO_2-based device (Figure 3c). This implies that interfacial recombination is reduced in the PDIN-based PVSC devices.

To gain an in-depth understanding of the influences of the PDIN on interfacial recombination and photovoltaic performance of the PVSCs, the dark J-V curves of a conventional PVSCs using the Shockley diode equation for a single junction device were modeled based on:

$$J_D = J_0 \left[exp\left(\frac{q\left(V - J_D R_S\right)}{nK_B T} \right) - 1 \right] \quad (1)$$

where J_0 is the reverse saturation current density, J_D is the dark current density, V is the applied bias, ^{q} is the electron charge, K_B is the Boltzmann constant, T is the temperature, and n is the ideal factor of the real diode.[42] The obtained diode parameters such as n and J_0 for the studied PVSCs are summarized in Table 1. The smaller values of n and J_0 were obtained for the FTO/PDIN-based device compared with those of the FTO/TiO_2-based device, and this proves that the PDIN possesses a better electron selectivity, and results in a decreased charge recombination loss at the ETL/perovskite interface. [43]

Figure 3d shows the dependence of photocurrent and photovoltage characteristics on the light intensity for the studied PDIN-based PVSCs. The results can be used to probe the recombination mechanisms which affect the device performance. From literature, the electroluminescence and photoluminescence emission spectroscopic analysis on the PVSCs showed that the bimolecular recombination is much weaker and not dominant the performance of PVSCs, whereas the interfacial recombination which occurs at the contacts between perovskite and ETLs or HTLs is dominant for their performance.[44] In contrast to results obtained in the short-circuit condition, in an open-circuit condition, all photo-generated charge carriers recombine and no current is extracted, thus the recombination mechanisms can be interpreted from the relationship between the measured values of V_{OC} and the light intensity. Based on the results of V_{OC} as a function of logarithmic irradiation light intensity (as shown in Fig X? Where is the figure???), the PDIN-based device has a low value of slope (1.45) compared to that of the TiO_2-based device (1.67). This indicates that the PDIN as an effective ETL can significantly mitigate the recombination loss at the ETL/perovskite interfaces. In principle, the relationship between V_{OC} versus light intensity (with a

slope of kT/q) corresponds to bimolecular recombination. A slope larger than the value of kT/q means that an additional interfacial trap-assisted Shockley-Read-Hall (SRH) recombination is involved.[45] A monomolecular recombination refers to any first order process including the geminate recombination of a bound electron-hole pair before dissociation and the SRH recombination at the shallow traps created by defects and impurities in the interfacial layer, whereas the bimolecular recombination is closely related to the recombination of free electrons and holes in the photoactive layer.[46] In order to reduce the interfacial recombination, a highly uniform planar perovskite thin film is essential for the absence of carrier traps. Therefore many methods have been used to produce high-quality perovskite thin films, including vapor deposition, two-step sequential solution deposition, vapor-assisted two-step reaction process or one-step solvent-induced fast crystallization-deposition.[1, 3, 47-49]

It is noted that the FTO/PDIN-based PVSCs possess a weaker V_{OC} dependence on the light intensity ($1.45K_BT/q$) than that of the FTO/TiO_2-based device ($1.67\ K_BT/q$) throughout the entire light intensity range. Under the short-circuit condition, the device shows super linearity of photocurrent with light density, reflecting that the charge collection of the FTO/PDIN-based PVSCs is independent of light-intensity. In this study, since we used the exactly same protocol for fabricating the $MAPbI_{3-x}Cl_x$ layer, there is no apparent difference in morphology of perovskite thin films with different substrates as shown in Figure S4. Therefore, we attributed this discrepancy in the light intensity dependence to the hole-blocking and passivation effects of the PDIN. This result also confirms that the PDIN ETL can effectively reduce the interfacial trap-assisted recombination, which is critical to increase value of the V_{OC} as well as improve the device performance.

In order to further understand the electronic transport?? processes at the perovskite/ETLs interfaces, electronic impedance spectroscopy (EIS) measurement was performed with an applied voltage at V_{OC} under illumination with an LED array emitting white light. Three elements are readily identified in the obtained Nyquist plot (Figure 4a) and Bode plot (Figure 4b) for both the PDIN- and TiO_2-based devices, indicating similar interfacial charge transport? processes. Figure 4c presents the

variation of interfacial resistance with the applied bias, which was derived from the data in the high frequency region in EIS characterization (in Fig. XX?). Though the PDIN based PVSC has a less conductivity value (0.8×10^{-5} S cm^{-1}) than that of high-temperature TiO_2 device (1.1×10^{-5} S cm^{-1}),[50] it is interesting to find that the interfacial resistance of the PDIN-based device is slightly smaller than that of TiO_2 one, which should be attributed to the passivation effects from the PDIN, thus resulting in a faster electron extraction. Due to the reduction of electron trap density due to passivation of ?? by ??, a smaller value of capacitance was obtained from the response in the intermediate frequency region in the EIS (see Fig. 4d). for the PDIN-based device when compared to that of TiO_2-based device. This reduction of the capacitance surely will benefit to increase the values of $V_{OC,}$ J_{SC} and FF for the PDIN-based device.

From the above results, it can be concluded that the PDIN is a very promising ETL that can be used to achieve a better performance for the standard PVSCs. Due to its low-temperature solution process, it is possible to fabricate flexible solar cells on polymer substrates. Herein, we replaced the rigid glass/FTO substrate with a flexible PET/ITO substrate and fabricated the devices via the same procedures. The optical transmittance and absorption spectra for the device on the flexible substrate are shown in Figure 5a. The transmittance of the PET/ITO/PDIN is similar to that of the glass/FTO/PDIN. However, a much less transmittance in the range between 450 and 600 nm was observed for the PET/ITO/PDIN. In order to clarify the reason for this, we obtained the optical absorbance spectrum of $MAPbI_{3-x}Cl_x$ based on such substrate in this spectral region and the results are shown in Figure 5a. Clearly there is no apparent decrease in the region. Figure 5b and 5c show such type of the flexible device and its J-V characteristics. In the J-V tests, the scan rate of applied voltage was kept at the same value of 20 mV per step with a delay time of 0.005 s. A champion PCE of 11.24% for a reverse scan was obtained, indicating a good performance of such flexible PVSCs (J_{SC}: 17.05 mA/cm^2, V_{OC}: 1.03 V and FF: 0.64). The analysis results from IPCE spectrum for the flexible PVSCs showed an efficiency of 84% at 400 nm (Figure 5d). Such a low IPCE value in the range of 600-800 nm can be

attributed to the smaller absorption of the perovskite in this spectral region (Figure 5a). Moreover, the flexible devices were bent repeatedly for 20 times to determine the flexibility and the test results are shown in Figure 5c. Clearly there is no apparent reduction of the performance after 20 cycles, i.e., the values of the J_{SC} and V_{OC} remain almost identical although the fill factor decreases slightly from 0.64 to 0.61. This demonstrates that our flexible devices can be tolerated well with the mechanical bending deformation. From the histogram of the PCE and hysteretic behavior of the flexible device shown in Figure S5, the flexible device exhibits slightly larger hysteresis effect compared with the rigid device based on PDIN as shown in Figure S6. This could be due to the higher series resistance of the flexible devices.

3. CONCLUSION

In summary, we have demonstrated that the PDIN can be used as an outstanding solution processable ETL for a standard PVSCs fabricated on both rigid and flexible substrates. Its deep valence band and the passivation effect of the terminal amino group as well as good electron-transport mobility are benefited from perylene diimide backbone, and this can effectively extract electron and block holes to reduce charge recombination loss at the ETL/perovskite interfaces. Its unique dipole moment and solution process capability enable the FTO/PDIN-based devices to perform much better than the control FTO-based device , with a promising PCE of 16.17% and 11.24% in rigid and flexible substrates, respectively. These results reveal the great potential of using PDIN ETL for the standard PVSCs and expand the present range of available ETL layer to small molecular semiconductors.

4. EXPERIMENTAL DETAILS

Device Fabrication Fluorine-doped tin oxide ($F:SnO_2$) coated glass (Pilkington TEC 15, 15 Ω/square) was patterned by etching with Zn powder and 2 M HCl diluted in milliQ water. The flexible PET/ITO was etched with 0.1 M HCl diluted in milliQ

water without Zn powder. The etched substrates were cleaned with 2% hellmanex diluted in milliQ water, rinsed with milliQ water/ethanol, and then dried with clean air. For the FTO/PDIN-based device, PDIN was dissolved in methanol with the assistance of acetic acid (2% in volume). To optimize the PDIN thickness, solutions of methanol and PDIN at varied concentrations (from 2 mg mL^{-1} to 8 mg mL^{-1}) were then spin-deposited onto FTO substrate at 3000 rpm for 30 s and then annealed at 100 ºC for 10 min. For the perovskite layer, 9 mg CH_3NH_3Cl was added in 1 ml of 45 wt% concentration of the $CH_3NH_3PbI_3$ solution and stirred for 4 hours at 50 ºC, then the $CH_3NH_3PbI_{3-x}Cl_x$ solution was dropped onto a PDIN coated FTO substrate. The substrate was then spun at 5000 rpm for six seconds, and then anhydrous chlorobenzene (200 μL) was quickly dropped onto the center of the substrate. The obtained films were dried at 100°C for 10 min. The hole-transport material was deposited by spin coating at 4000 rpm for 30 s. The spin coating solution was prepared by dissolving 72.3 mg spiro-MeOTAD, 17.5 μL of a stock solution of 520 mg mL^{-1} lithium bis(trifluoromethylsulphonyl)imide in acetonitrile and 28.8 μL 4-tert-butylpyridine in 1 mL chlorobenzene. Device fabrication was finally completed by thermal evaporation of a 70-nm-thick film of gold as the cathode. To compred with, a control FTO/TiO_2-based device and flexible device based on the PDIN were prepared following the above processes. (Here you need to list the main differencs!) All device fabrication was carried out in a dry air-filled glove box and a humidity of <1.0 ppm.

Samples Characterization A solar simulator with a Xe light source (450 W, Oriel, model 9119) and an AM 1.5G filter (Oriel, model 91192) was used to give an irradiance of 100 mW cm^{-2} on the surface of the solar cell. The current-voltage characteristics of the cell were obtained by applying an external potential bias to the cell and measuring the photocurrent generated under these conditions using a Keithley model 2400 digital source meter (USA). A similar data-acquisition system was used to control the photon-to-current response (internal quantum efficiency, IQE) measurements. A white-light bias of 10% solar intensity was applied onto the sample during the IQE measurements, which employed a monochromatic light modulated at

10 Hz. Steady-state photoluminescence (PL) was measured using Horiba Jobin Yvon system with an excitation laser beam at 532 nm. X-ray diffraction (XRD) experiments were conducted using a Philips X-ray diffractometer with Cu Kα radiation. The samples were scanned from 10° to 70° with a step-size of 0.02°. Impedance spectra (IS) were collected with an Autolab Frequency Analyzer setup consisting of the Autolab PGSTAT 30 (Eco Chemie B.V., Utrecht, The Netherlands) and the Frequency Response Analyzer module. The measurements were performed at around V_{OC} ± 0.2V (via tuning the bias light intensity with white LED light radiation) in the frequency range 0.01 Hz-1 MHz with oscillation potential amplitudes of 30 mV. The obtained impedance spectra were fitted using Z-view software (v2.8b, Scribner Associates Inc.).

5. ACKNOWLEDGEMENTS

Financial support from the National Basic Research Program of China (2014CB643506 and 2013CB922104), the Director Fund of the Wuhan National Laboratory for Optoelectronics, Wuhan National High Magnetic Field Center (PHMFF2015018), and Royal Academy of Engineering-Research Exchange with China and India is gratefully acknowledged.

Conflict of Interest:
The authors declare no competing financial interest.

SUPPORTING INFORMATION

This material is available free of charge via the Internet at http://pubs.acs.org.

REFERENCES

1. Burschka, J.; Pellet, N.; Moon, S.; Humphry-Baker, R.; Gao, P.; Nazeeruddin, M. K.; Grätzel, M. *Nature* **2013**, *499*, 316.
2. Zhou, H.; Chen, Q.; Li, G.; Luo, S.; Song, T.; Duan, H-S.; Hong, Z.; You, J.; Liu, Y.; Yang, Y. *Science* **2014**, *345*, 542.
3. Liu, M.; Johnston, M. B.; Snaith, H. J. *Nature* **2013**, *501*, 395.

4. Mei, A.; Li, X.; Liu, L.; Ku, Z.; Liu, T.; Rong,Y.; Xu,M.; Hu, M.; Chen, J.; Yang, Y.; Grätzel, M.; Han, H. *Science* **2014**, *345*, 295.
5. Yang, W.; Noh, J.; Jeon, N.; Kim, Y.; Ryu, S.; Seo, J.; Seok, S. *Science*, **2015**, *348*, 6240.
6. Bi, D. Q.; Yang, L.; Boschloo, G.; Hagfeldt, A.; Johansson, E. M. J. *J. Phys. Chem. Lett.* **2013**, *4*, 1532.
7. O'Regan, B.; Gratzel, M. *Nature* **1991**, *353*, 737.
8. Kumar, M. H.; Yantara, N.; Dharani, S.; Graetzel, M.; Mhaisalkar, S.; Boix, P. P.; Mathews, N. *Chem. Commun*., **2013**, *49*, 11089.
9. Bi, D.; Boschloo, G.; Schwarzmüller, S.; Yang, L.; Johanssona, E. M. J.; Hagfeldt, A. *Nanoscale*, **2013**, *5*, 11686.
10. Dong, J.; Zhao, Y.; Shi, J.; Wei, H.; Xiao, J.; Xu, X.; Luo, J.; Xu, J.; Li, D.; Luo, Y.; Meng, Q. *Chem. Commun*., **2014**,*50*, 13381.
11. Mahmood, K.; Swain, B. S.; Jung, H. S. *Nanoscale*, **2014**, *6*, 9127.
12. Kim, J.; Kim, G.; Kim, T. K.; Kwon, S.; Back, H.; Lee, J.; Lee, S. H.; Kang, H.; Lee, K. *J. Mater. Chem. A*, **2014**, *2*, 17291.
13. Son, D.; Im, J-K.; Kim, H-S.; Park, N-G. *J. Phys. Chem. C* **2014**, *118*, 16567.
14. Liu, D.; Kelly, T. L. *Nature Photon*. **2014**, *8*, 133.
15. Sun, S.; Wu, P.; Xing, P. *Appl. Phys. Lett.* **2012**, *101*, 132417.
16. Scanlon,D. O.; Regoutz, A.; Egdell, R. G.; Morgan, D. J.; Watson, G. W. *Appl. Phys. Lett.* **2013**,*103*, 262108.
17. Mu, J.; Chen, B.; Zhang, M.; Guo, Z.; Zhang, P.; Zhang, Z.; Sun, Y.; Shao, C.; Liu, Y. *ACS Appl. Mater. Interfaces* **2012**, *4*, 424.
18. Liang, C.; Meng, G.; Lei, Y.; Phillipp, F.; Zhang, L. *Adv. Mater*. **2001**, 13, 1330.
19. Brennan, T. P.; Tanskanen, J. T.; Roelofs, K. E.; To, J. W. F.; Nguyen, W. H.; Bakke, J .R.; Ding, I-K.; Hardin, B. E.; Sellinger, A.; McGehee, M.D.; Bent, S. F. W. H. *J. Phys. Chem. C* **2013**, *117*, 24138.
20. Gan, J.; Lu, X.; Wu, J.; Xie, S.; Zhai, T.; Yu, M.; Zhang, Z.; Mao, Y.; Wang, S. C.; Shen, Y.; Tong, Y. *Sci Rep*, **2013**, *3*, 1021.
21. Dong, Q.; Shi, Y.; Wang, K.; Li, Y.; Wang, S.; Zhang, H.; Xing, Y.; Du, Y.; Bai, X.; Ma, T. *J. Phys. Chem. C* **2015**, *119*, 10212.
22. Song, J.; Zheng, E.; Bian, J.; Wang, X-F.; Tian, W.; Sanehirac, Y.; Miyasakac, T. *J. Mater. Chem. A*, **2015**, *3*, 10837.
23. Dong, W.; Meng, T.; Chen, Q. *SCI ADV MATER*, **2015**, *7*, 120.
24. Ke, W.; Fang, G.; Liu, Q.; Xiong, L.; Qin, P.; Tao, H.; Wang, J.; Lei, H.; Li, B.; Wan, J.; Yang, G.; Yan, Y. *J. Am. Chem. Soc*. **2015**, *137*, 6730.
25. Desai, U. V.; Xu, C.; Wu, J.; Gao, D. *J. Phys. Chem. C* **2013**, *117*, 3232.
26. Hossain, M. A.; Jennings, J. R.; Koh, Z. Y.; Wang, Q. *ACS Nano* **2011**, *5*, 3172.
27. Zhu, Z.; Zheng, X.; Bai, Y.; Zhang, T.; Wang, Z.; Xiao, S.; Yang, S. *Phys.Chem.Chem.Phys*., **2015**, *17*, 18265.
28. Baena, J. P. C.; Steier, L.; Tress, W.; Saliba, M.; Neutzner, S.; Matsui, T.; Giordano, F.; Jacobsson, T. J.; Kandada, A. R. S.; Zakeeruddin, S. M.; Petrozza, A.; Abate, A.; Nazeeruddin, M. K.; Grätzel, M.; Hagfeldt, A. *Energy Environ. Sci*., **2015**, 8, 2928-2934.
29. Ong, B. S.; Li, C. S.; Li, Y. N.; Wu, Y. L.; Loutfy, R. *J. Am. Chem. Soc.* **2007**, 129, 2750.
30. Beiley, Z. M.; McGehee, M. D. *Energy Environ. Sci*. **2012**, 5, 9173.

31. Wang, J. T-W.; Ball, J. M.; Barea, E. M.; Abate, A.; Alexander-Webber,J. A.; Huang, J.; Saliba, M.; Mora-Sero,I.; Bisquert, J.; Snaith,H. J.; Nicholas, R. J. *Nano Lett.* **2014**, *14*, 724.
32. Cao, D. H.; Stoumpos, C. C.; Malliakas,C. D.; Katz, M. J.; Farha,O. K.; Hupp,J. T.; Kanatzidis, M. J. *APL Mater.* **2014**, *2*, 091101.
33. Ke, W.; Fang, G.; Wan, J.; Tao, H.; Liu, Q.; Xiong, L.; Qin, P.; Wang, J.; Lei, H.; Yang, G.; Qin, M.; Zhao, X.; Yan, Y. *Nat. Commun*., **2015**, *6*, 6700.
34. Zhang, Z-G.; Qi, B.; Jin, Z.; Chi, D.; Qi, Z.; Li, Y.; Wang, J. *Energy Environ. Sci*., **2014**, *7*, 1966.
35. Min, J.; Zhang, Z-G.; Hou, Y.; Quiroz, C. O. R.; Przybilla, T.; Bronnbauer, C.; Guo, F.; Forberich, K.; Azimi, H.; Ameri, T.; Spiecker, E.; Li, Y.; Brabec, C. J. *Chem. Mater*., **2015**, 27 (1), 227-234.
36. Yip, H.-L.; Jen, A. K. Y. *Energy Environ. Sci*., **2012**, *5*, 5994.
37. Kim, H.-S.; Lee, C.-R.; Im, J.-H.; Lee, K.-B.;Moehl, T.; Marchioro, A.; Moon, S.-J.; Humphry-Baker, R.; Yum, J.-H.; Moser, J. E.; Grätzel, M.;Park, N-G. *Sci. Rep*. **2012**, 2, 591.
38. Shao, Y. ; Xiao, Z. ; Bi, C.; Yuan, Y. ; Huang, J. *Nat. Commun*. **2014**, 5, 5784.
39. Sun, C.; Wu, Z.; Yip, H-L.; Zhang, H.; Jiang, X-F.; Xue, Q.; Hu, Z.; Hu, Z.; Shen, Y.; Wang, M.; Huang, F.; Cao, Y. *Adv. Energy Mater.* DOI: 10.1002/aenm.201501534
40. Liang, P.-W.; Chueh, C.-C. ; Xin, X.-K. ; Zuo, F.; Williams, S. T.; Liao, C.-Y. ; Jen, A. K. Y. *Adv. Energy. Mater.* **2015**, 5, 1400960.
41. Choi, H.; Mai, C.-K.; Kim, H.-B.; Jeong, J.; Song, S.; Bazan, G. C.; Kim, J. Y.; Heeger, A. J. *Nat. Commun.* 2015, 6, 7348.
42. Kyaw, A. K. K.; Wang, D. H.; Gupta, V.; Leong, W. L.; Ke, L.; Bazan, G. C.; Heeger, A. J. *ACS Nano,* **2013**, *7*, 4569.
43. Zang, Y.; Li, C. Z.; Chueh, C. C.; Williams, S. T.; Jiang, W.; Wang, Z. H.; Yu, J. S.; Jen, A. K.-Y. *Adv. Mater*, **2014**, *26*, 5708.
44. Tress, W.; Marinova, N.; Inganäs, O.; Nazeeruddin, M. K.; Zakeeruddin, S. M.; Grätzel, M. *Adv. Energy Mater.* **2014**, 1400812.
45. van Duren, J. K. J.; Yang, X.; Loos, J.; Bulle-Lieuwma, C. W. T.; Sieval, A. B.; Hummelen, J. C.; Janssen, R. A. J. *Adv. Funct. Mater*. **2004**, *14*, 425.
46. You, J.; Yang, Y. (M.); Hong, Z.; Song, T.-B.; Meng, L.; Liu, Y.; Jiang, C.; Zhou, H.; Chang, W.-H.; Li, G.; Yang, Y. *Appl. Phys. Lett*. **2014**, *105*, 183902.
47. Chen, Q.; Zhou, H.; Hong, Z. R.; Luo, S.; Duan, H.-S.; Wang, H.-H.; Liu, Y. S.; Li, G.; Yang, Y. *J. Am. Chem. Soc*. **2014**, *136*, 622.
48. Jeon, N. J.; Noh, J. H.; Kim,Y. C.; Yang, W. S.; Ryu, S.; Seok, S. I. *Nat. Materials*, 2014, 13, 897.
49. Xiao, M.; Huang, F.; Huang, W.; Dkhissi, Y.; Zhu, Y.; Etheridge, J.; Gray-Weale, A.; Bach, U.; Cheng, Y-B.; Spiccia, L. *Angew. Chem. Int. Ed.* **2014**, *53*, 1.
50. Wojciechowski, K.; Saliba, M.; Leijtens, T.; Abate, A.; Snaith, H. J. *Energy Environ. Sci*., **2015**, 8, 2928.

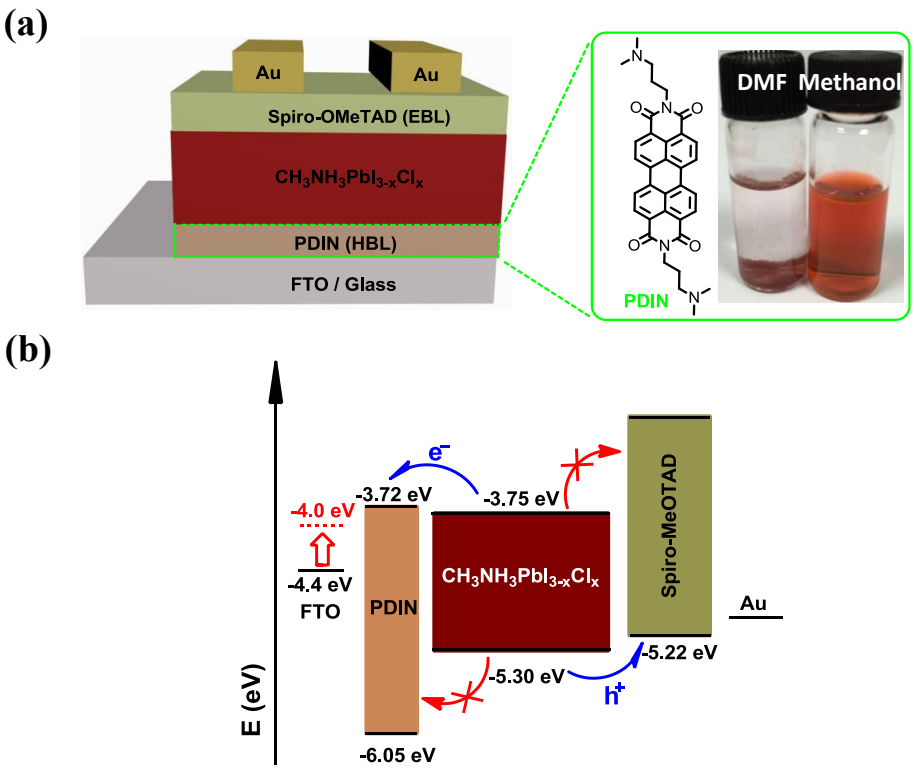

Figure 1. (a) Device architecture of the regular PVSCs and molecular structures of the PDIN used for device fabrication, as well as the investigation of its solubility in N, N-Dimethyl-formamide and methanol, (b) The corresponding energy band diagram relative to vacuum level.

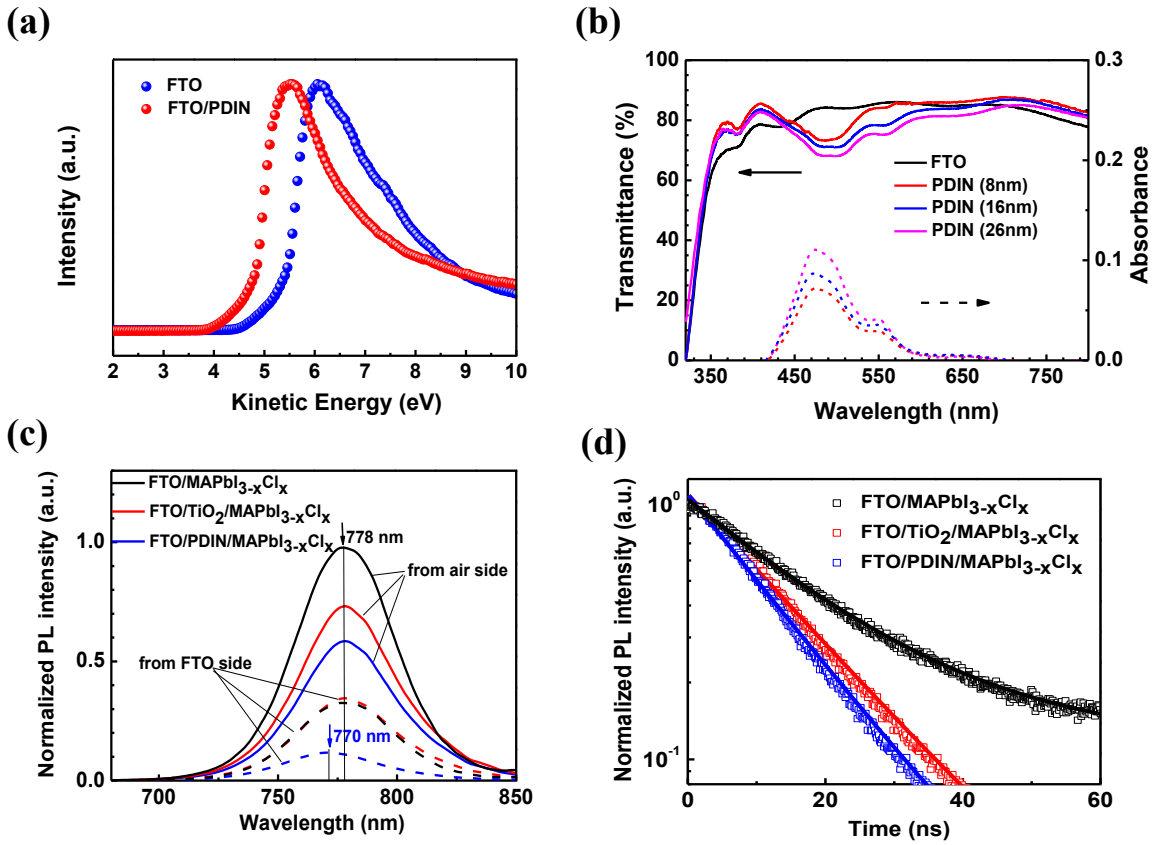

Figure 2. (a) UPS spectra of the FTO and FTO/PDIN substrates, the obtained Fermi level for FTO and FTO/PDIN is 4.4 eV and 4.0 eV respectively, (b) Absorption (right) and transmittance (left) spectra of PDIN thin films, (c) The steady-state photoluminescence spectra of $MAPbI_{3-x}Cl_x$ films on different substrates with an excitation wavelength of 532 nm from the FTO side and the air side, (d) time-resolved PL decay of $MAPbI_{3-x}Cl_x$ film on the different substrates.

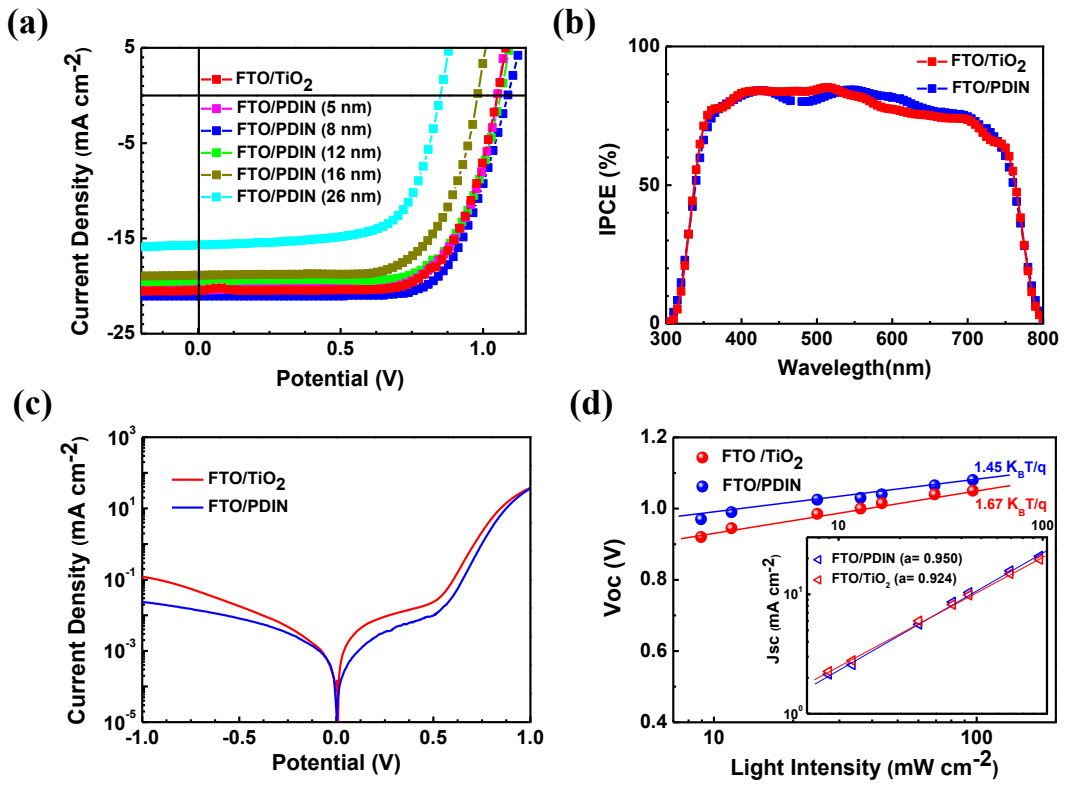

Figure 3. (a) J-V curves of the PVSCs based on FTO/PDIN with different thicknesses and the reference device based on the FTO/TiO_2, using a metallic mask with an aperture area of 0.08 cm^2. The applied voltage scan rate in J-V measurement was kept at the same 20 mV per step with a delay time of 0.005 s in reverse scan direction. The optimal thicknesses of PDIN is 8 nm, (b) IPCE spectra of the optimized FTO/PDIN-based device and the reference device, (c) J-V curves of the optimized FTO/PDIN-based device and the reference device under dark condition, (d) V_{OC} dependence and J_{SC} dependence (inset) upon different light intensity for the optimized FTO/PDIN-based device and the reference device.

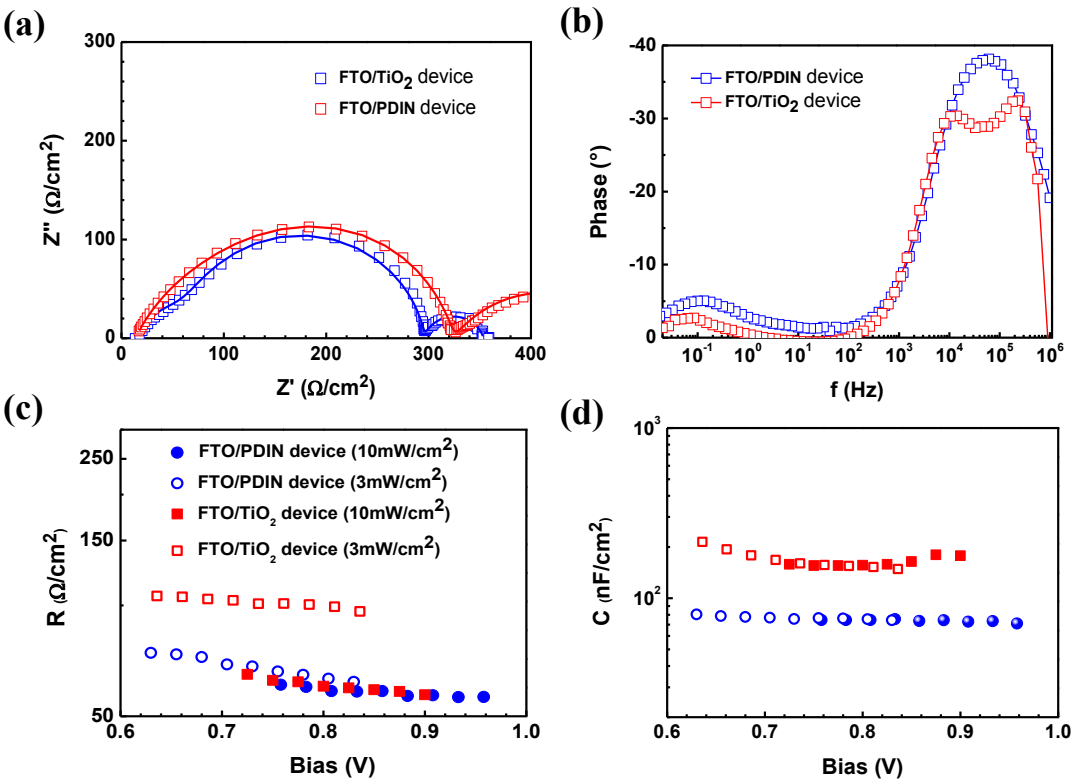

Figure 4. Impedance spectroscopy of perovskite solar cell with different ETLs was performed at around V_{OC} under illumination with an LED array emitting white light, the applied voltage of 0.9 V is given as an example (a) in the form of Nyquist plot, (b) in the form of Bode plot, (c) the interfacial resistance derived from high frequency region as a function of the applied voltage, (d) the capacitance derived from the intermediate frequency region as a function of the applied voltage.

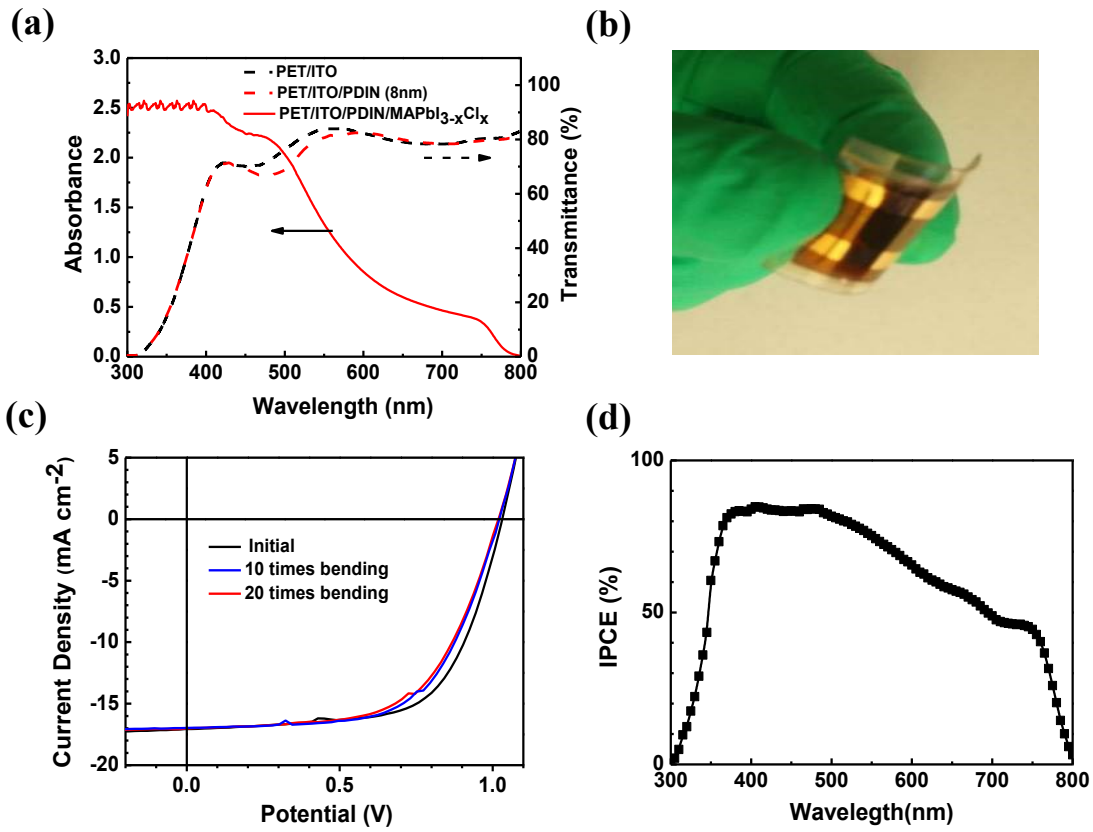

Figure 5. (a) Absorption (left) and transmittance (right) spectra of the films based on flexible PET/ITO substrate, (b) a photograph of the flexible device based PDIN, (c) the current-voltage (J-V) characteristics of the flexible device, using a metallic mask with an aperture area of 0.08 cm^2, while the scan rate was kept at 20 mV per step with a delay time of 0.005 s in reverse scan direction. The J-V performance after bending is also included in it (d) IPCE spectra of the flexible device based PDIN.

Table 1 Device parameters of the PVSCs based on the FTO/TiO_2 and FTO/PDIN under the illumination of AM 1.5G, 100 mW cm^2

Substrate	V_{OC} (V)	J_{SC} (mA/cm^2)	FF (%)	PCE_{max} (PCE_{ave}[a]) (%)	n[b]	J_0[b] (mA/cm^2)
TiO_2/FTO	1.05	20.45	0.70	15.03 (14.85)	1.48	6.4×10^{-8}
PDIN/FTO	1.08	20.80	0.72	16.17 (15.56)	1.32	2.1×10^{-8}

[a] The average PCE is obtained from over 20 devices. [b] Extracted from the dark J-V curves.

Table 2 Device parameters of the PVSCs based on PDIN/FTO with various PDIN thicknesses under the illumination of AM 1.5G, 100 mW cm^2

HBL layer	Thickness (nm)	V_{OC} (V)	J_{SC} (mA/cm^2)	FF (%)	PCE (%)	R_S (Ω/cm^2)
PDIN	5	1.05	20.42	0.69	14.79	2.24
	8	1.08	20.80	0.72	16.17	2.01
	12	1.06	19.47	0.70	14.44	2.43
	16	0.98	18.87	0.68	12.57	3.36
	26	0.85	15.67	0.67	8.92	4.58